On Some Rigorous Computational Ocean–Acoustic Modelling Tools

David W. Bartel
Maritime Operations Division
Defence Science and Technology Organisation
Adelaide, South Australia
Email: david.bartel@dsto.defence.gov.au

***Abstract*— This paper discusses four computer programs developed by the author for use within the Defence Science and Technology Organisation: `HANKEL`, a range–independent transmission loss model based on the wavenumber–integral method; `Multi_LP`, a tool for computing the complex reflection coefficient for plane wave incidence upon a seafloor boundary where the seafloor is comprised of a stack of uniform sediment layers overlying a uniform basement; and two time–series simulation models, `DPRAY`, for range–independent environments, and `WEDGE`, for a wedge. The main emphasis with each code is on mathematical rigour and quantitative exploration of the physics.**

I. Introduction

Much effort has been expended over recent decades on ocean–acoustic modelling [1]–[4]. Many computer models exist for ocean–acoustic calculations, such as those freely available for download from the Ocean Acoustics Library web site [5]. Despite the availability of such well–respected models as `KRAKEN`, `ORCA`, `RAM`, `BELLHOP` and `OASES`, there still exist valid reasons for developing other models in–house. One major reason is that there may be a requirement for a particular calculation that is not readily supplied by available models, such as producing the time history of the Doppler shift on each multipath within a ray tracing calculation. In such a situation it may be simpler and easier to write a model from scratch that is designed to produce just the desired output.

Another reason to create an in–house model arises from the need to interface an ocean–acoustic model with an existing engineering system, such as a torpedo or a naval combat system, which typically have very tight computational resource constraints. For these systems it may be better to produce a fast, simple model from scratch that is expressly built to focus solely on those ocean–acoustic calculations that are most salient to the current tactical requirements. Existing models, which are typically designed for stand–alone use by an individual at his or her workstation, may simply be too unwieldy to use effectively in the context of automated tactical naval software. At the very least a layer of translation software may need to be written to provide an interface between the ocean–acoustic model and the engineering system.

Writing an ocean–acoustic model oneself may also provide a pedagogical benefit—learning by doing. The theory of computational ocean–acoustics is complex and available treatments are often heavily mathematical [3], [4]. Existing computer codes range from the relatively simple, as in `RAM`, to the complex, such as `ORCA`. One way to learn about the art of ocean–acoustic modelling, and of some of the phenomena of underwater acoustic propagation, is to simply create one's own models and explore their output. This exercise might be useful even if the model never leaves the laboratory. By writing a model one gains insight into what other computer codes are trying to do, and an understanding of some of the pitfalls to be avoided in such codes, such as taking the wrong branch of a complex square root. This experience may prove of benefit when interpreting the output of a well–known computer model, since it could be assumed that any given model might occasionally produce erroneous results under some circumstances. Then again, when writing a model from scratch, one is free to do things differently from what other widely available models have done, and perhaps radically so.

The four computer models discussed in this paper, `HANKEL`, `Multi_LP`, `DPRAY` and `WEDGE`, were written by the author for several of the reasons given above. `HANKEL` was written as an attempt to gain more insight into the physics of propagation in a plane–parallel waveguide consisting of homogeneous acoustic media. To that end, `HANKEL` creates scripts that allow an electronic report to be automatically generated. This report is in the form of a PDF document, and it illustrates the integrands involved in calculating the complex pressure at a given receiver location. `Multi_LP` was written to provide a benchmark–quality model for computing the plane wave reflection coefficient, using multiple–precision to avoid numerical pitfalls that have tended to plague this type of calculation. This tool was designed to provide an independent check on the output of other widely available models such as `BOUNCE` (available from the Ocean Acoustics Library [5]). `DPRAY` was written as a prototype for an in–house ray tracing model, `MODRAY`, using an algorithm that promised to be quite useful [6]. `DPRAY` illustrates the exact calculation of the Doppler shift, at every sampling instant and along every multipath, in an ocean–acoustic environment where the speed of sound may vary with depth and where sources and receivers may undergo manoeuvres. Lastly, `WEDGE` was written to explore the physics of propagation within a beach–like environment. Accurate Doppler calculations are incorporated in `WEDGE`, allowing a high–fidelity time series to be synthesized for a moving source and receiver. Each model is discussed further in sections II–V.

978-1-4244-5222-4/10/$26.00 ©2010 CROWN

II. HANKEL

A computer program, HANKEL, was written by the author to compute the complex acoustic pressure field within a horizontally–stratified ocean–acoustic environment, based upon the *Hankel transform* method of solution of the Helmholtz equation [4]. A uniform ocean, with speed of sound $c_0\,\mathrm{m{\cdot}s^{-1}}$, occupies the region $\{(x, y, z) : 0 < z < h\}$, where h is the ocean depth. The ocean surface $\{(x, y, z) : z = 0\}$ is assumed to be a perfect reflector, with surface reflection coefficient $R_S = -1$; the bottom $\{(x, y, z) : z > h\}$ is assumed to be horizontally–stratified (having material properties varying only with depth z), characterised solely by its complex bottom reflection coefficient R_B (see section III). In cylindrical (r, z) coordinates we have a point source S at $(0, z_S)$ and one or more point receivers R at (r, z_R), where $0 < z_S < h$ and $0 \le z_R \le h$. The source emits a unit–amplitude spherical wave of angular frequency $\omega\,\mathrm{rad{\cdot}s^{-1}}$ and time dependence $e^{-i\omega t}$. The wavenumber in water for the tone emitted by S is $k = \omega/c_0$, with horizontal and vertical components k_r and k_z, respectively, satisfying $k_r^2 + k_z^2 = k^2$, where $0 < k < \infty$, $0 \le k_r < \infty$, and k_z is either purely real ($k_z = \sqrt{k^2 - k_r^2}$), if $k_r \le k$, or purely imaginary ($k_z = i\sqrt{k_r^2 - k^2}$), if $k_r > k$.

The starting point for HANKEL is equation (6.31) of Frisk [4], which gives the pressure $p = p(r, z_R)$ as an infinite series of definite integrals, *viz.*

$$
\begin{aligned}
p &= \sum_{n=0}^{\infty} \sum_{\ell=1}^{4} p_{\ell n} \\
&= \sum_{n=0}^{\infty} \int_0^{\infty} \left(t_{1n} + t_{2n} + t_{3n} + t_{4n}\right) J_0\left(k_r r\right)\, k_r\, dk_r, \quad (1)
\end{aligned}
$$

with

$$t_{1n} = \frac{i}{k_z} e^{ik_z|z_R - z_S|} \left(R_S R_B\right)^n e^{2ink_z h}, \quad (2)$$

$$t_{2n} = \frac{i}{k_z} R_B e^{ik_z[2h-(z_R+z_S)]} \left(R_S R_B\right)^n e^{2ink_z h}, \quad (3)$$

$$t_{3n} = \frac{i}{k_z} R_S e^{ik_z(z_R+z_S)} \left(R_S R_B\right)^n e^{2ink_z h}, \quad \text{and} \quad (4)$$

$$t_{4n} = \frac{i}{k_z} R_B R_S e^{ik_z[2h-|z_R-z_S|]} \left(R_S R_B\right)^n e^{2ink_z h}, \quad (5)$$

where $J_0(.)$ is the Bessel function of the first kind of order 0.

The formulation (1)–(5) is based upon the decomposition of a spherical wave into a *spectrum* of plane waves over horizontal wavenumber $0 \le k_r < \infty$ [3, §26.3]. Each integral $p_{\ell n}$ in (1) may be considered to be a kind of *generalised ray* [4, §6.3.1]. For $n = 0$, for instance, we have the terms

$$p_{10} = \int_0^{\infty} \frac{i}{k_z} e^{ik_z|z_R-z_S|} J_0\left(k_r r\right)\, k_r\, dk_r, \quad (6)$$

$$p_{20} = \int_0^{\infty} \frac{i}{k_z} R_B e^{ik_z[2h-(z_R+z_S)]} J_0\left(k_r r\right)\, k_r\, dk_r, \quad (7)$$

$$p_{30} = \int_0^{\infty} \frac{i}{k_z} R_S e^{ik_z(z_R+z_S)} J_0\left(k_r r\right)\, k_r\, dk_r, \quad \text{and} \quad (8)$$

$$p_{40} = \int_0^{\infty} \frac{i}{k_z} R_B R_S e^{ik_z[2h-|z_R-z_S|]} J_0\left(k_r r\right)\, k_r\, dk_r. \quad (9)$$

p_{10} is a generalisation of the direct ray path of classical geometrical acoustics; p_{20} of the ray path with a single bottom bounce (hence the bottom reflection coefficient R_B in (7)); p_{30} of the ray path with a single top bounce (hence the surface reflection coefficient R_S in (8)); and p_{40} of the ray path with a single bottom bounce followed by a single top bounce (hence the product $R_B R_S$ in (9)) [4, Fig. 6.2]. For each higher value of n we add one more cycle of bottom and top reflections to the plane waves of the previous n. Thus p_{11} is a generalisation of the ray path with a single top bounce followed by a single bottom bounce; p_{21} of the ray path with a bottom bounce, then a top bounce, then a second bottom bounce; p_{31} of the ray path with a top bounce, then a bottom bounce, then a second top bounce; and so on. Note that these classical rays will propagate in a direction given by a wavenumber vector $\mathbf{k} = (k_r, k_z)$ where k_z is real—the generalised rays in (1) include *all* plane waves with positive k_r, including those with *imaginary* k_z corresponding to *inhomogeneous* plane waves [7]. Classical ray tracing only includes homogeneous waves.

Defining a complex propagation angle $\theta = \Re(\theta) + i\Im(\theta)$, with $k_r = k \sin\theta$ and $k_z = k \cos\theta$, we transform (1) into

$$
\begin{aligned}
p = \sum_{n=0}^{\infty} \int_0^{\frac{\pi}{2} - i\infty} & \left(u_{1n} + u_{2n} + u_{3n} + u_{4n}\right) \\
& \times J_0\left(kr \sin\theta\right) \left(k \sin\theta\right) \left(k \cos\theta\right) d\theta, \quad (10)
\end{aligned}
$$

with

$$u_{1n} = \frac{i}{k\cos\theta} e^{i(k\cos\theta)|z_R-z_S|} \left(R_S R_B\right)^n u, \quad (11)$$

$$u_{2n} = \frac{i}{k\cos\theta} R_B e^{i(k\cos\theta)[2h-(z_R+z_S)]} \left(R_S R_B\right)^n u, \quad (12)$$

$$u_{3n} = \frac{i}{k\cos\theta} R_S e^{i(k\cos\theta)(z_R+z_S)} \left(R_S R_B\right)^n u, \quad \text{and} \quad (13)$$

$$u_{4n} = \frac{i}{k\cos\theta} R_B R_S e^{i(k\cos\theta)[2h-|z_R-z_S|]} \left(R_S R_B\right)^n u, \quad (14)$$

where

$$u = e^{2in(k\cos\theta)h}, \quad (15)$$

$$R_S \equiv R_S(\theta), \quad \text{and} \quad (16)$$

$$R_B \equiv R_B(\theta). \quad (17)$$

The contour integrals throughout (10) are to be interpreted as over $C = C_1 \cup C_2$, where $C_1 = \{\theta \in \mathbb{C} : 0 \le \Re(\theta) \le \frac{\pi}{2}, \Im(\theta) = 0\}$ and $C_2 = \{\theta \in \mathbb{C} : \Re(\theta) = \frac{\pi}{2}, -\infty < \Im(\theta) < 0\}$. C_1 covers the range of real propagation angles $0 \le \Re(\theta) \le \frac{\pi}{2}$, where $\Re(\theta) = 0$ applies to propagation in the vertical direction (up or down), while $\Re(\theta) = \frac{\pi}{2}$ applies to horizontal propagation. C_2 is associated with evanescent waves [3], [4]. We need to include C_2 to provide the full solution to the Helmholtz equation.

Write the complex bottom reflection coefficient $R_B(\theta)$ in polar form,

$$R_B(\theta) = \left|R_B\left(\theta\right)\right| e^{i\Phi_B(\theta)}, \quad (18)$$

where $|R_B(\theta)|$ is the magnitude and $\Phi_B(\theta)$ is the phase, respectively. With these substitutions, (10) becomes

$$\begin{aligned}
p = {} & ik \sum_{n=0}^{\infty} (-1)^n \int_0^{\frac{\pi}{2}-i\infty} v_{1n} J_0(kr\sin\theta)\sin\theta\, d\theta \\
& + ik \sum_{n=0}^{\infty} (-1)^n \int_0^{\frac{\pi}{2}-i\infty} v_{2n} J_0(kr\sin\theta)\sin\theta\, d\theta \\
& + ik \sum_{n=0}^{\infty} (-1)^{n+1} \int_0^{\frac{\pi}{2}-i\infty} v_{3n} J_0(kr\sin\theta)\sin\theta\, d\theta \\
& + ik \sum_{n=0}^{\infty} (-1)^{n+1} \int_0^{\frac{\pi}{2}-i\infty} v_{4n} J_0(kr\sin\theta)\sin\theta\, d\theta,
\end{aligned} \tag{19}$$

where

$$v_{1n} = |R_B(\theta)|^n e^{i(2nh+|z_R-z_S|)k\cos\theta} e^{in\Phi_B(\theta)}, \tag{20}$$

$$v_{2n} = |R_B(\theta)|^{n+1} e^{i[2(n+1)h-(z_R+z_S)]k\cos\theta} e^{i(n+1)\Phi_B(\theta)}, \tag{21}$$

$$v_{3n} = |R_B(\theta)|^n e^{i(2nh+z_R+z_S)k\cos\theta} e^{in\Phi_B(\theta)}, \quad \text{and} \tag{22}$$

$$v_{4n} = |R_B(\theta)|^{n+1} e^{i[2(n+1)h-|z_R-z_S|]k\cos\theta} e^{i(n+1)\Phi_B(\theta)}. \tag{23}$$

Parameterize C_2 as $C_2 = \{\pi/2 - ia \in \mathbb{C} : a > 0\}$, so that integrals in θ over $(\pi/2, \pi/2 - i\infty)$ are expressed as integrals in a over $(0, \infty)$. Further, using the identities

$$e^{i\phi} = \cos\phi + i\sin\phi, \tag{24}$$

$$\cos(\pi/2 - ia) = i\sinh a, \quad \text{and} \tag{25}$$

$$\sin(\pi/2 - ia) = \cosh a, \tag{26}$$

we expand (19) into 24 infinite series of definite–integral expressions as follows. (This formulation is convenient since the zeroes of $\cos(z_\ell k\cos\theta)$, $\sin(z_\ell k\cos\theta)$, $\ell \in \{1, ..., 4\}$, $J_0(kr\sin\theta)$ and $J_0(kr\cosh a)$ are easily obtained, and quadrature (numerical integration) may be applied between each pair of adjacent zeroes—`HANKEL` uses this method. The author is unaware of any previous publication of these formulae explicitly in the literature, so they are provided here in full.)

$$\begin{aligned}
p = {} & ik \sum_{n=0}^{\infty} (-1)^n \int_0^{\pi/2} |R_B(\theta)|^n \cos(z_1 k\cos\theta) \\
& \quad \times \cos(n\Phi_B(\theta)) J_0(kr\sin\theta)\sin\theta\, d\theta \\
& + k \sum_{n=0}^{\infty} (-1)^{n+1} \int_0^{\pi/2} |R_B(\theta)|^n \cos(z_1 k\cos\theta) \\
& \quad \times \sin(n\Phi_B(\theta)) J_0(kr\sin\theta)\sin\theta\, d\theta \\
& + k \sum_{n=0}^{\infty} (-1)^{n+1} \int_0^{\pi/2} |R_B(\theta)|^n \sin(z_1 k\cos\theta) \\
& \quad \times \cos(n\Phi_B(\theta)) J_0(kr\sin\theta)\sin\theta\, d\theta \\
& + ik \sum_{n=0}^{\infty} (-1)^{n+1} \int_0^{\pi/2} |R_B(\theta)|^n \sin(z_1 k\cos\theta) \\
& \quad \times \sin(n\Phi_B(\theta)) J_0(kr\sin\theta)\sin\theta\, d\theta \\
& + ik \sum_{n=0}^{\infty} (-1)^n \int_0^{\infty} |R_B(\pi/2 - ia)|^n e^{-z_1 k\sinh a} \\
& \quad \times \cos(n\Phi_B(\pi/2 - ia)) J_0(kr\cosh a)\cosh a\, da \\
& + k \sum_{n=0}^{\infty} (-1)^{n+1} \int_0^{\infty} |R_B(\pi/2 - ia)|^n e^{-z_1 k\sinh a} \\
& \quad \times \sin(n\Phi_B(\pi/2 - ia)) J_0(kr\cosh a)\cosh a\, da \\
& + ik \sum_{n=0}^{\infty} (-1)^n \int_0^{\pi/2} |R_B(\theta)|^{n+1} \cos(z_2 k\cos\theta) \\
& \quad \times \cos((n+1)\Phi_B(\theta)) J_0(kr\sin\theta)\sin\theta\, d\theta \\
& + k \sum_{n=0}^{\infty} (-1)^{n+1} \int_0^{\pi/2} |R_B(\theta)|^{n+1} \cos(z_2 k\cos\theta) \\
& \quad \times \sin((n+1)\Phi_B(\theta)) J_0(kr\sin\theta)\sin\theta\, d\theta \\
& + k \sum_{n=0}^{\infty} (-1)^{n+1} \int_0^{\pi/2} |R_B(\theta)|^{n+1} \sin(z_2 k\cos\theta) \\
& \quad \times \cos((n+1)\Phi_B(\theta)) J_0(kr\sin\theta)\sin\theta\, d\theta \\
& + ik \sum_{n=0}^{\infty} (-1)^{n+1} \int_0^{\pi/2} |R_B(\theta)|^{n+1} \sin(z_2 k\cos\theta) \\
& \quad \times \sin((n+1)\Phi_B(\theta)) J_0(kr\sin\theta)\sin\theta\, d\theta \\
& + ik \sum_{n=0}^{\infty} (-1)^n \int_0^{\infty} |R_B(\pi/2 - ia)|^{n+1} e^{-z_2 k\sinh a} \\
& \quad \times \cos((n+1)\Phi_B(\pi/2 - ia)) J_0(kr\cosh a)\cosh a\, da \\
& + k \sum_{n=0}^{\infty} (-1)^{n+1} \int_0^{\infty} |R_B(\pi/2 - ia)|^{n+1} e^{-z_2 k\sinh a} \\
& \quad \times \sin((n+1)\Phi_B(\pi/2 - ia)) J_0(kr\cosh a)\cosh a\, da \\
& + ik \sum_{n=0}^{\infty} (-1)^{n+1} \int_0^{\pi/2} |R_B(\theta)|^n \cos(z_3 k\cos\theta) \\
& \quad \times \cos(n\Phi_B(\theta)) J_0(kr\sin\theta)\sin\theta\, d\theta \\
& + k \sum_{n=0}^{\infty} (-1)^n \int_0^{\pi/2} |R_B(\theta)|^n \cos(z_3 k\cos\theta) \\
& \quad \times \sin(n\Phi_B(\theta)) J_0(kr\sin\theta)\sin\theta\, d\theta \\
& + k \sum_{n=0}^{\infty} (-1)^n \int_0^{\pi/2} |R_B(\theta)|^n \sin(z_3 k\cos\theta) \\
& \quad \times \cos(n\Phi_B(\theta)) J_0(kr\sin\theta)\sin\theta\, d\theta \\
& + ik \sum_{n=0}^{\infty} (-1)^n \int_0^{\pi/2} |R_B(\theta)|^n \sin(z_3 k\cos\theta) \\
& \quad \times \sin(n\Phi_B(\theta)) J_0(kr\sin\theta)\sin\theta\, d\theta \\
& + ik \sum_{n=0}^{\infty} (-1)^{n+1} \int_0^{\infty} |R_B(\pi/2 - ia)|^n e^{-z_3 k\sinh a} \\
& \quad \times \cos(n\Phi_B(\pi/2 - ia)) J_0(kr\cosh a)\cosh a\, da \\
& + k \sum_{n=0}^{\infty} (-1)^n \int_0^{\infty} |R_B(\pi/2 - ia)|^n e^{-z_3 k\sinh a} \\
& \quad \times \sin(n\Phi_B(\pi/2 - ia)) J_0(kr\cosh a)\cosh a\, da
\end{aligned}$$

$$
\begin{aligned}
&+ ik \sum_{n=0}^{\infty} (-1)^{n+1} \int_0^{\pi/2} |R_B(\theta)|^{n+1} \cos(z_4 k \cos\theta) \\
&\quad \times \cos((n+1)\Phi_B(\theta)) J_0(kr\sin\theta) \sin\theta \, d\theta \\
&+ k \sum_{n=0}^{\infty} (-1)^{n} \int_0^{\pi/2} |R_B(\theta)|^{n+1} \cos(z_4 k \cos\theta) \\
&\quad \times \sin((n+1)\Phi_B(\theta)) J_0(kr\sin\theta) \sin\theta \, d\theta \\
&+ k \sum_{n=0}^{\infty} (-1)^{n} \int_0^{\pi/2} |R_B(\theta)|^{n+1} \sin(z_4 k \cos\theta) \\
&\quad \times \cos((n+1)\Phi_B(\theta)) J_0(kr\sin\theta) \sin\theta \, d\theta \\
&+ ik \sum_{n=0}^{\infty} (-1)^{n} \int_0^{\pi/2} |R_B(\theta)|^{n+1} \sin(z_4 k \cos\theta) \\
&\quad \times \sin((n+1)\Phi_B(\theta)) J_0(kr\sin\theta) \sin\theta \, d\theta \\
&+ ik \sum_{n=0}^{\infty} (-1)^{n+1} \int_0^{\infty} |R_B(\pi/2 - ia)|^{n+1} e^{-z_4 k \sinh a} \\
&\quad \times \cos((n+1)\Phi_B(\pi/2 - ia)) J_0(kr\cosh a) \cosh a \, da \\
&+ k \sum_{n=0}^{\infty} (-1)^{n} \int_0^{\infty} |R_B(\pi/2 - ia)|^{n+1} e^{-z_4 k \sinh a} \\
&\quad \times \sin((n+1)\Phi_B(\pi/2 - ia)) J_0(kr\cosh a) \cosh a \, da,
\end{aligned} \tag{27}
$$

where

$$z_1 = 2nh + |z_R - z_S|, \tag{28}$$
$$z_2 = 2(n+1)h - (z_R + z_S), \tag{29}$$
$$z_3 = 2nh + z_R + z_S, \quad \text{and} \tag{30}$$
$$z_4 = 2(n+1)h - |z_R - z_S|. \tag{31}$$

Each of the integrals appearing throughout (27) is now real and may be evaluated by standard quadrature methods. Note that the integrals over $a \in (0, \infty)$ are converted into integrals over $\theta \in (0, \pi)$ by the transformation $a = \cot^2(\theta/2)$. Adaptive interval halving and convergence checking is used, where QUADPACK routine DQXGS is applied to each panel [8]. We note that the only approximations used in HANKEL are those involved in the numerical evaluation of the most significant definite integrals in (27), and that the solution produced by HANKEL is intended to be a good numerical approximation of the exact solution (27).

Figs. 1 and 2 illustrate transmission loss surfaces computed by HANKEL by simple ray tracing and by the exact solution (27). The underlying problem is an extension of that given in Schmidt and Jensen [9], and it consists of a shallow ocean of depth $100\,\mathrm{m}$, speed of sound $1500\,\mathrm{m{\cdot}s^{-1}}$ and density $1000\,\mathrm{kg{\cdot}m^{-3}}$ overlying a solid halfspace, of density $2000\,\mathrm{kg{\cdot}m^{-3}}$, compressional speed $1800\,\mathrm{m{\cdot}s^{-1}}$, shear speed $600\,\mathrm{m{\cdot}s^{-1}}$, compressional attenuation $0.1\,\mathrm{dB}/\lambda_\mathrm{p}$ and shear attenuation $0.2\,\mathrm{dB}/\lambda_\mathrm{s}$. We have a source at depth $95\,\mathrm{m}$ emitting a pure $30\,\mathrm{Hz}$ tone. The transmission loss is computed out to $3\,\mathrm{km}$ and throughout the water column. Note the presence of fine ripples in the surface in Fig. 2 which are absent in Fig. 1. Schmidt and Jensen state that these ripples are created by an interference pattern arising from the superposition of a single waterborne mode and an interface wave known as a *Scholte* wave [9]. HANKEL implicitly includes Scholte waves because it performs a direct numerical approximation of the exact full–field solution (27).

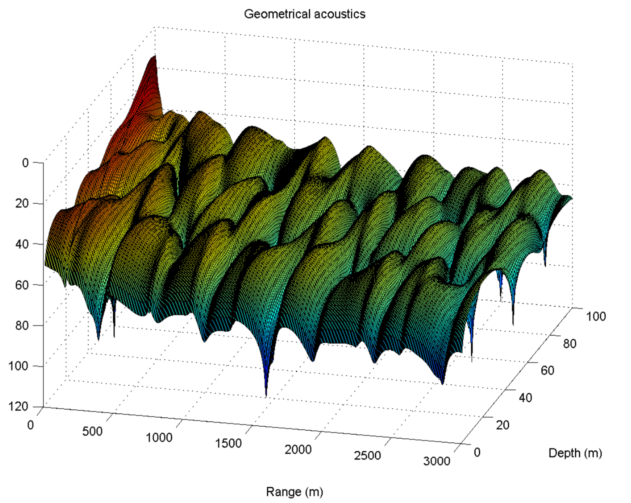

Fig. 1. Transmisison loss surface at 30 Hz, in decibels, computed by a simple ray tracing method.

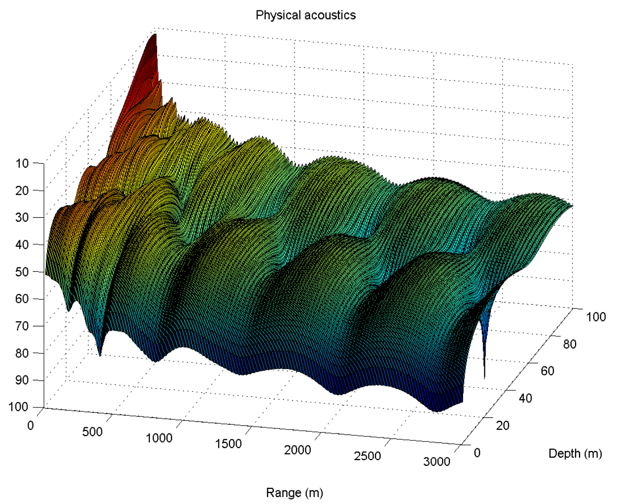

Fig. 2. Transmisison loss surface at 30 Hz, in decibels, computed by the wavenumber integration method.

A novel feature of HANKEL, setting it apart from other wavenumber–integral models known to the author such as OASES, RPRESS and SCOOTER, is a facility for the creation of an electronic report, in Portable Document Format (PDF). This report illustrates both the traditional Green's function and the most significant integrands involved in the calculation of the field at a given receiver point and for a given source frequency. HANKEL uses the supplied runtime parameters to create a MATLAB script file that, when run, creates a set of labelled Encapsulated Postscript (EPS) and JPEG files for each of the integrands and their multiplicative component parts. In addition, HANKEL produces a LaTeX source file that, when processed, produces the PDF report with each figure having a caption that describes the mathematical form of the associated integrand. This documentation aid is of potential use by both the student and experienced acoustician alike in understanding the detailed physics of the full–field solution in a simple range–independent environment.

Figs. 3 and 4 illustrate this 'auto–documentation' feature of HANKEL. The EPS files for these figures were created by running the MATLAB script created by HANKEL, and the associated captions were copied and pasted directly from the LaTeX script file that HANKEL produced. The problem associated with Figs. 3 and 4 involved an ocean of depth $100\,\mathrm{m}$, density $1000\,\mathrm{kg{\cdot}m^{-3}}$ and speed of sound $1500\,\mathrm{m{\cdot}s^{-1}}$ overlying a solid halfspace, of density $2000\,\mathrm{kg{\cdot}m^{-3}}$, compressional speed $1800\,\mathrm{m{\cdot}s^{-1}}$, shear speed $600\,\mathrm{m{\cdot}s^{-1}}$, compressional attenuation $0.7\,\mathrm{dB}/\lambda_{\mathrm{p}}$ and shear attenuation $1.5\,\mathrm{dB}/\lambda_{\mathrm{s}}$. A source at depth $25\,\mathrm{m}$ emitted a pure tone of frequency $100\,\mathrm{Hz}$ and the complex pressure p was synthesized at the field point at range $100\,\mathrm{m}$ and depth $5\,\mathrm{m}$. The transmission loss was estimated to be about $41.41\,\mathrm{dB}$.

Fig. 3 is a plot of the magnitude $|g(k_r)|$ of the Green's function $g(k_r)$ for the sample problem discussed above, where [4, (6.18)]

$$\begin{aligned} & k_z\left(1 - R_S R_B e^{2ik_z h}\right) g(k_r) \\ & = i\left[e^{ik_z|z_R - z_S|} + R_S e^{ik_z(z_R+z_S)}\right] \\ & + iR_B e^{2ik_z h}\left[e^{-ik_z(z_R+z_S)} + R_S e^{-ik_z|z_R-z_S|}\right]. \qquad (32) \end{aligned}$$

Note that the model OASES [10] computes the pressure p directly from the Green's function, since an alternative formulation to (1) is ([4, (6.19)])

$$p = \int_0^\infty g(k_r)\, J_0(k_r r)\, k_r\, dk_r. \qquad (33)$$

HANKEL uses the form (27) to explore the generalised ray interpretation.

Fig. 4 is a plot of the integrand 'f4ss' (from the 22nd series in (27)) for the sample problem, *viz.*

$$\begin{aligned} & \frac{2\pi}{15}\,|R_B(\theta)| \sin(\Phi_B(\theta)) \\ & \times \sin(24\pi\cos\theta)\, J_0\left(\frac{40\pi}{3}\sin\theta\right)\sin\theta. \qquad (34) \end{aligned}$$

Term 1 in Fig. 4 is

$$\frac{2\pi}{15}\,|R_B(\theta)| \sin(\Phi_B(\theta))\,; \qquad (35)$$

term 2 is

$$\sin(24\pi\cos\theta)\,; \qquad (36)$$

and term 3 is

$$J_0\left(\frac{40\pi}{3}\sin\theta\right)\sin\theta. \qquad (37)$$

Note that the correspondence between classical and generalised rays is drawn out in Fig. 4 by marking the propagation angle of the classical ray associated with the particular generalised ray integral of which (34) is the integrand.

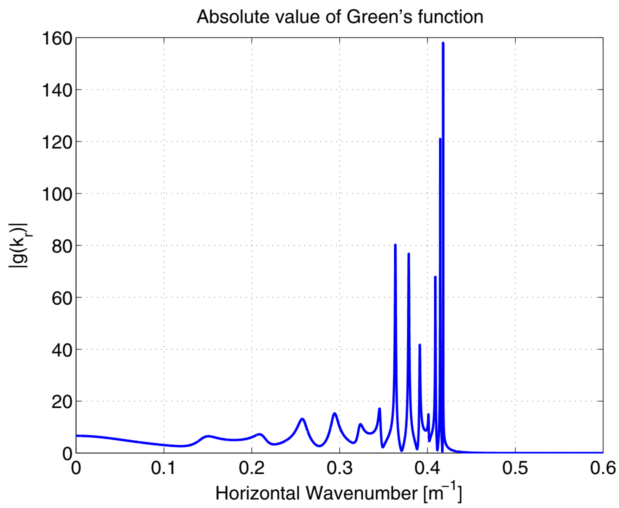

Fig. 3. Absolute value $|g(k_r)|$ of the Green's function $g(k_r)$ as a function of horizontal wavenumber k_r.

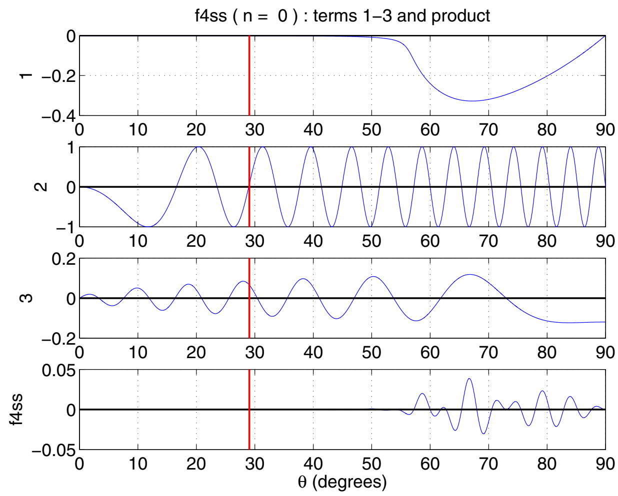

Fig. 4. Multiplicative terms in "f4ss" (which is the pointwise product of terms 1, 2 and 3). The vertical red line marks the propagation angle of the associated classical ray.

III. MULTI_LP

Multi_LP deals with plane wave reflection in homogeneous acoustic media. We have two halfspaces, one a fluid and the other a solid. There are, optionally, one or more homogeneous solid layers separating the two halfspaces. A plane wave is assumed to be propagating in the fluid halfspace towards the solid halfspace (or the first solid layer, if there are any), and Multi_LP computes the plane wave reflection coefficient for the wave that is reflected back into the fluid halfspace.

More precisely, suppose we have a plane wave of the form $\exp[i(k_{0z}z - k_{0x}x - \omega t)]$ propagating in a homogeneous fluid halfspace of density ρ_0 kg.m^{-3}, sound speed c_0 m.s^{-1} and attenuation $\alpha_0\,\mathrm{dB}/\lambda_0$, where $\lambda_0 = \omega/c_0$ is the wavelength of the plane wave. Let the fluid halfspace occupy the region $\{(x,y,z) : z < 0\}$ of three–dimensional space $\mathbb{R}^3$.

By a suitable rotation of axes we ensure that the intersection of the plane wave with the interface plane $z = 0$ is parallel to the y axis. Suppose a second halfspace, a homogeneous solid, occupies the region $\{(x, y, z) : \delta < z < \infty\}$ for some $\delta \geq 0$. Let this solid medium have density ρ_{n+1} kg.m^{-3}, compressional speed $c_{(n+1)p}$ m.s^{-1}, shear speed $c_{(n+1)s}$ m.s^{-1}, compressional attenuation $\alpha_{(n+1)\mathrm{p}}\,\mathrm{dB}/\lambda_{(n+1)\mathrm{p}}$ and shear attenuation $\alpha_{(n+1)\mathrm{s}}\,\mathrm{dB}/\lambda_{(n+1)\mathrm{s}}$, where $\lambda_{(n+1)p} = \omega/c_{(n+1)p}$ and $\lambda_{(n+1)s} = \omega/c_{(n+1)s}$ are wavelengths of the compressional and shear waves, respectively, that propagate in the solid halfspace, for the given source wave of angular frequency ω rad.s^{-1}. Let the gap between the fluid and solid halfspaces be filled with $n \in \{0, 1, ...\}$ homogeneous solid media. If $n = 0$, we just have the two halfspaces filling $\mathbb{R}^3$, with no gap between them. For $n \in \{1, 2, ...\}$, however, let medium $j \in \{1, ..., n\}$ occupy $\{(x, y, z) : d_1 + ... + d_{j-1} < z < d_1 + ... + d_j\}$, where we set $d_1 + ... + d_{j-1} = 0$ by definition when $j = 1$. We suppose medium $j \in \{1, ..., n\}$ to have density ρ_j kg.m^{-3}, compressional speed c_{jp} m.s^{-1}, shear speed c_{js} m.s^{-1}, compressional attenuation $\alpha_{\mathrm{jp}}\,\mathrm{dB}/\lambda_{\mathrm{jp}}$ and shear attenuation $\alpha_{\mathrm{js}}\,\mathrm{dB}/\lambda_{\mathrm{js}}$, where $\lambda_{jp} = \omega/c_{jp}$ and $\lambda_{js} = \omega/c_{js}$ are the wavelengths of the compressional and shear waves, respectively, that propagate in layer j.

The problem that `Multi_LP` addresses is the calculation of the plane wave reflection coefficient r^{pp} for the wave $r^{pp} \exp[-i(k_{0z}z + k_{0x}x + \omega t)]$ that is reflected from the boundary $\{(x, y, z) : z = 0\}$ and back into medium 0. The general solution is obtained from solving a set of $4n + 3$ linear equations in $4n + 3$ unknowns r^{pp}, A_j, B_j, C_j, D_j, t^{pp} and t^{ps}, $j \in \{1, ..., n\}$ [11]. We obtain the solution by observing the requirement of continuity of horizontal and vertical particle velocity and stress components across media interfaces, following the treatment in Ainslie [11]. These equations are given explicitly as follows (the author is unaware of any previous occurrence of this explicit formulation in the ocean–acoustics literature, so it is provided here in full).

For $n = 0$ we have the following three equations in the three unknowns r^{pp}, t^{pp}, t^{ps}:

$$k_{0z}r^{pp} + k_{1pz}t^{pp} - k_{0x}t^{ps} = k_{0z}, \tag{38}$$

$$2k_{0x}k_{1pz}t^{pp} + \left(k_{1sz}^2 - k_{0x}^2\right)t^{ps} = 0, \quad \text{and} \tag{39}$$

$$\lambda_0 k_0^2 r^{pp} - \left(\lambda_1 k_{1p}^2 + 2\mu_1 k_{1pz}^2\right)t^{pp} + 2\mu_1 k_{0x}k_{1sz}t^{ps} = -\lambda_0 k_0^2. \tag{40}$$

For $n = 1$ we have the following seven equations in the seven unknowns r^{pp}, A_1, B_1, C_1, D_1, t^{pp}, t^{ps}:

$$k_{0z}r^{pp} + k_{1pz}A_1 - k_{1pz}B_1 - k_{0x}C_1 - k_{0x}D_1 = k_{0z}, \tag{41}$$

$$2k_{0x}k_{1pz}A_1 - 2k_{0x}k_{1pz}B_1 + \left(k_{1sz}^2 - k_{0x}^2\right)C_1 + \left(k_{1sz}^2 - k_{0x}^2\right)D_1 = 0, \tag{42}$$

$$\lambda_0 k_0^2 r^{pp} - \left(\lambda_1 k_{1p}^2 + 2\mu_1 k_{1pz}^2\right)A_1 - \left(\lambda_1 k_{1p}^2 + 2\mu_1 k_{1pz}^2\right)B_1 + 2\mu_1 k_{0x}k_{1sz}C_1 - 2\mu_1 k_{0x}k_{1sz}D_1 = -\lambda_0 k_0^2, \tag{43}$$

$$k_{0x}\exp(ik_{1pz}d_1)A_1 + k_{0x}\exp(-ik_{1pz}d_1)B_1 + k_{1sz}\exp(ik_{1sz}d_1)C_1 - k_{1sz}\exp(-ik_{1sz}d_1)D_1 - k_{0x}t^{pp} - k_{2sz}t^{ps} = 0, \tag{44}$$

$$k_{1pz}\exp(ik_{1pz}d_1)A_1 - k_{1pz}\exp(-ik_{1pz}d_1)B_1 - k_{0x}\exp(ik_{1sz}d_1)C_1 - k_{0x}\exp(-ik_{1sz}d_1)D_1 - k_{2pz}t^{pp} + k_{0x}t^{ps} = 0, \tag{45}$$

$$2\mu_1 k_{0x}k_{1pz}\exp(ik_{1pz}d_1)A_1 - 2\mu_1 k_{0x}k_{1pz}\exp(-ik_{1pz}d_1)B_1 + \mu_1\left(k_{1sz}^2 - k_{0x}^2\right)\exp(ik_{1sz}d_1)C_1 + \mu_1\left(k_{1sz}^2 - k_{0x}^2\right)\exp(-ik_{1sz}d_1)D_1 - 2\mu_2 k_{0x}k_{2pz}t^{pp} - \mu_2\left(k_{2sz}^2 - k_{0x}^2\right)t^{ps} = 0, \quad \text{and} \tag{46}$$

$$\left(\lambda_1 k_{1p}^2 + 2\mu_1 k_{1pz}^2\right)\exp(ik_{1pz}d_1)A_1 + \left(\lambda_1 k_{1p}^2 + 2\mu_1 k_{1pz}^2\right)\exp(-ik_{1pz}d_1)B_1 - 2\mu_1 k_{0x}k_{1sz}\exp(ik_{1sz}d_1)C_1 + 2\mu_1 k_{0x}k_{1sz}\exp(-ik_{1sz}d_1)D_1 - \left(\lambda_2 k_{2p}^2 + 2\mu_2 k_{2pz}^2\right)t^{pp} + 2\mu_2 k_{0x}k_{2sz}t^{ps} = 0. \tag{47}$$

For $n \in \{2, 3, ...\}$ we have the following $4n + 3$ equations in the $4n + 3$ unknowns r^{pp}, A_j, B_j, C_j, D_j, t^{pp} and t^{ps}, $j \in \{1, ..., n\}$:

$$k_{0z}r^{pp} + k_{1pz}A_1 - k_{1pz}B_1 - k_{0x}C_1 - k_{0x}D_1 = k_{0z}, \tag{48}$$

$$2k_{0x}k_{1pz}A_1 - 2k_{0x}k_{1pz}B_1 + \left(k_{1sz}^2 - k_{0x}^2\right)C_1 + \left(k_{1sz}^2 - k_{0x}^2\right)D_1 = 0, \tag{49}$$

$$\lambda_0 k_0^2 r^{pp} - \left(\lambda_1 k_{1p}^2 + 2\mu_1 k_{1pz}^2\right)A_1 - \left(\lambda_1 k_{1p}^2 + 2\mu_1 k_{1pz}^2\right)B_1 + 2\mu_1 k_{0x}k_{1sz}C_1 - 2\mu_1 k_{0x}k_{1sz}D_1 = -\lambda_0 k_0^2, \tag{50}$$

$$k_{0x}\exp\left(ik_{(\ell-1)pz}d_{\ell-1}\right)A_{\ell-1} + k_{0x}\exp\left(-ik_{(\ell-1)pz}d_{\ell-1}\right)B_{\ell-1} + k_{(\ell-1)sz}\exp\left(ik_{(\ell-1)sz}d_{\ell-1}\right)C_{\ell-1} - k_{(\ell-1)sz}\exp\left(-ik_{(\ell-1)sz}d_{\ell-1}\right)D_{\ell-1} - k_{0x}A_\ell - k_{0x}B_\ell - k_{\ell sz}C_\ell + k_{\ell sz}D_\ell = 0, \quad \ell \in \{2, 3, ..., n\}, \tag{51}$$

$$k_{(\ell-1)pz}\exp\left(ik_{(\ell-1)pz}d_{\ell-1}\right)A_{\ell-1} - k_{(\ell-1)pz}\exp\left(-ik_{(\ell-1)pz}d_{\ell-1}\right)B_{\ell-1} - k_{0x}\exp\left(ik_{(\ell-1)sz}d_{\ell-1}\right)C_{\ell-1} - k_{0x}\exp\left(-ik_{(\ell-1)sz}d_{\ell-1}\right)D_{\ell-1} - k_{\ell pz}A_\ell + k_{\ell pz}B_\ell + k_{0x}C_\ell + k_{0x}D_\ell = 0, \quad \ell \in \{2, 3, ..., n\}, \tag{52}$$

$$2\mu_{\ell-1}k_{0x}k_{(\ell-1)pz}\exp\left(ik_{(\ell-1)pz}d_{\ell-1}\right)A_{\ell-1} - 2\mu_{\ell-1}k_{0x}k_{(\ell-1)pz}\exp\left(-ik_{(\ell-1)pz}d_{\ell-1}\right)B_{\ell-1} + \mu_{\ell-1}\left(k_{(\ell-1)sz}^2 - k_{0x}^2\right)\exp\left(ik_{(\ell-1)sz}d_{\ell-1}\right)C_{\ell-1} + \mu_{\ell-1}\left(k_{(\ell-1)sz}^2 - k_{0x}^2\right)\exp\left(-ik_{(\ell-1)sz}d_{\ell-1}\right)D_{\ell-1} - 2\mu_\ell k_{0x}k_{\ell pz}A_\ell + 2\mu_\ell k_{0x}k_{\ell pz}B_\ell - \mu_\ell\left(k_{\ell sz}^2 - k_{0x}^2\right)C_\ell - \mu_\ell\left(k_{\ell sz}^2 - k_{0x}^2\right)D_\ell = 0, \quad \ell \in \{2, 3, ..., n\}, \tag{53}$$

$$\left(\lambda_{\ell-1}k_{(\ell-1)p}^2 + 2\mu_{\ell-1}k_{(\ell-1)pz}^2\right)\exp\left(ik_{(\ell-1)pz}d_{\ell-1}\right)A_{\ell-1} + \left(\lambda_{\ell-1}k_{(\ell-1)p}^2 + 2\mu_{\ell-1}k_{(\ell-1)pz}^2\right) \times \exp\left(-ik_{(\ell-1)pz}d_{\ell-1}\right)B_{\ell-1}$$

$$
\begin{aligned}
&- 2\mu_{\ell-1} k_{0x} k_{(\ell-1)sz} \exp\left(ik_{(\ell-1)sz} d_{\ell-1}\right) C_{\ell-1} \\
&+ 2\mu_{\ell-1} k_{0x} k_{(\ell-1)sz} \exp\left(-ik_{(\ell-1)sz} d_{\ell-1}\right) D_{\ell-1} \\
&- \left(\lambda_\ell k_{\ell p}^2 + 2\mu_\ell k_{\ell pz}^2\right) A_\ell - \left(\lambda_\ell k_{\ell p}^2 + 2\mu_\ell k_{\ell pz}^2\right) B_\ell \\
&+ 2\mu_\ell k_{0x} k_{\ell sz} C_\ell - 2\mu_\ell k_{0x} k_{\ell sz} D_\ell = 0, \\
&\ell \in \{2, 3, ..., n\}, \qquad (54)
\end{aligned}
$$

$$
\begin{aligned}
&k_{0x} \exp\left(ik_{npz} d_n\right) A_n + k_{0x} \exp\left(-ik_{npz} d_n\right) B_n \\
&+ k_{nsz} \exp\left(ik_{nsz} d_n\right) C_n - k_{nsz} \exp\left(-ik_{nsz} d_n\right) D_n \\
&- k_{0x} t^{pp} - k_{(n+1)sz} t^{ps} = 0, \qquad (55)
\end{aligned}
$$

$$
\begin{aligned}
&k_{npz} \exp\left(ik_{npz} d_n\right) A_n - k_{npz} \exp\left(-ik_{npz} d_n\right) B_n \\
&- k_{0x} \exp\left(ik_{nsz} d_n\right) C_n - k_{0x} \exp\left(-ik_{nsz} d_n\right) D_n \\
&- k_{(n+1)pz} t^{pp} + k_{0x} t^{ps} = 0, \qquad (56)
\end{aligned}
$$

$$
\begin{aligned}
&2\mu_n k_{0x} k_{npz} \exp\left(ik_{npz} d_n\right) A_n \\
&- 2\mu_n k_{0x} k_{npz} \exp\left(-ik_{npz} d_n\right) B_n \\
&+ \mu_n \left(k_{nsz}^2 - k_{0x}^2\right) \exp\left(ik_{nsz} d_n\right) C_n \\
&+ \mu_n \left(k_{nsz}^2 - k_{0x}^2\right) \exp\left(-ik_{nsz} d_n\right) D_n \\
&- 2\mu_{n+1} k_{0x} k_{(n+1)pz} t^{pp} \\
&- \mu_{n+1} \left(k_{(n+1)sz}^2 - k_{0x}^2\right) t^{ps} = 0, \qquad (57)
\end{aligned}
$$

and

$$
\begin{aligned}
&\left(\lambda_n k_{np}^2 + 2\mu_n k_{npz}^2\right) \exp\left(ik_{npz} d_n\right) A_n \\
&+ \left(\lambda_n k_{np}^2 + 2\mu_n k_{npz}^2\right) \exp\left(-ik_{npz} d_n\right) B_n \\
&- 2\mu_n k_{0x} k_{nsz} \exp\left(ik_{nsz} d_n\right) C_n \\
&+ 2\mu_n k_{0x} k_{nsz} \exp\left(-ik_{nsz} d_n\right) D_n \\
&- \left(\lambda_{n+1} k_{(n+1)p}^2 + 2\mu_{n+1} k_{(n+1)pz}^2\right) t^{pp} \\
&+ 2\mu_{n+1} k_{0x} k_{(n+1)sz} t^{ps} = 0, \qquad (58)
\end{aligned}
$$

where wavenumber components k_{0x}, k_{0z}, k_{jpz} and k_{jsz} satisfy

$$k_{0x}^2 + k_{0z}^2 = k_0^2 = \left(\frac{\omega}{c_0}\right)^2 \left(1 + \alpha_0 \eta^{-1} i\right)^2, \qquad (59)$$

$$k_{jpz} = \left(k_{jp}^2 - k_{0x}^2\right)^{1/2}, \quad j \in \{1, 2, ..., n+1\}, \qquad (60)$$

$$k_{jsz} = \left(k_{js}^2 - k_{0x}^2\right)^{1/2}, \quad j \in \{1, 2, ..., n+1\}, \qquad (61)$$

$$k_{jp} = \frac{\omega}{c_{jp}} \left(1 + \alpha_{jp} \eta^{-1} i\right), \quad j \in \{1, 2, ..., n+1\}, \qquad (62)$$

$$k_{js} = \frac{\omega}{c_{js}} \left(1 + \alpha_{js} \eta^{-1} i\right), \quad j \in \{1, 2, ..., n+1\}, \qquad (63)$$

$$\eta = 40\pi \log_{10}(e). \qquad (64)$$

λ_j and μ_j are the Lamé coefficients for medium j [11].

Observe that the complex exponential terms appearing throughout (44)–(47) and (51)–(58) are, in general, of the form

$$\exp\left[\pm i\left(a + bi\right)\right] = \exp\left(\pm ia\right) \exp(\mp b), \qquad (65)$$

where $a \geq 0$ and $b \geq 0$. For $b \gg 0$, which occurs at high source frequency ω and/or for thick layers, $\exp(-b) \ll 1$ and $\exp(b) \gg 1$, a fact that makes the system of equations (41)–(47) or (48)–(58) ill–conditioned. To help avoid these well–known numerical difficulties, Lévesque and Piché provided a careful formulation of the solution that sidesteps the difficulties [12]. `Multi_LP` implements the algorithm of Lévesque and Piché, but adds further robustness in the form of using higher precision than standard double–precision, and a judicious treatment of the calculation of hyperbolic sines and cosines of a complex argument and large magnitude. This makes `Multi_LP` suitable for the accurate calculation of the plane wave reflection coefficient even for problems involving high source frequencies and thick layers. Moreover, `Multi_LP` creates a `MATLAB` script file that, when run, generates a set of labelled EPS and JPEG files for handy viewing of the results.

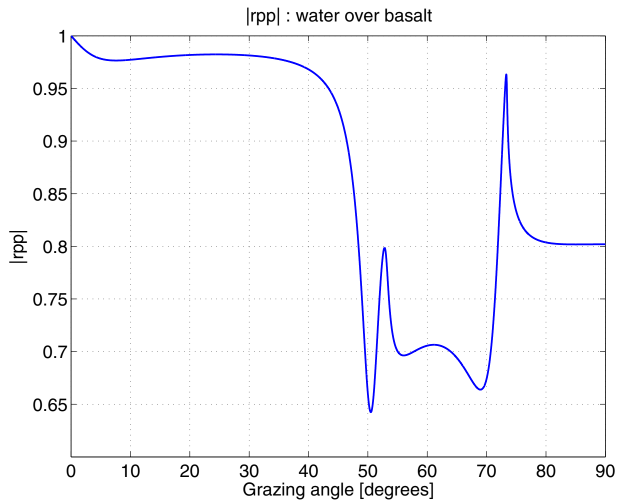

Fig. 5. Magnitude of bottom reflection coefficient for a water halfspace over a basalt halfspace.

Fig. 5 shows the magnitude of the bottom reflection coefficient for a sample problem computed with `Multi_LP`. The problem of Fig. 5 had a uniform ocean, of density $1000\,\mathrm{kg{\cdot}m^{-3}}$ and speed of sound $1500\,\mathrm{m{\cdot}s^{-1}}$ overlying a ‘basalt’ halfspace, of density $2600\,\mathrm{kg{\cdot}m^{-3}}$, compressional speed $5250\,\mathrm{m{\cdot}s^{-1}}$, shear speed $2500\,\mathrm{m{\cdot}s^{-1}}$, compressional attenuation $0.2\,\mathrm{dB}/\lambda_{1\mathrm{p}}$ and shear attenuation $0.5\,\mathrm{dB}/\lambda_{1\mathrm{s}}$.

IV. `DPRAY`

In acoustic ray tracing, one may be faced with the problem of determining the launch angle of a ray that leaves a given source and strikes a given receiver. This is an important problem when considering sources and receivers that are in motion throughout a simulation. `DPRAY` uses a method of Westwood and Vidmar to efficiently locate all eigenrays based upon the *Snell invariant* [6]. The environment assumed in `DPRAY` is range–independent, but the speed of sound in the water, $c(z)$, may vary with depth z. `DPRAY` uses a piecewise linear model for $c(z)$, for which Westwood and Vidmar provide the explicit formulae to be used in their algorithm.

`DPRAY` allows for sources, targets and receivers to move at smoothly–varying speeds and headings, but at fixed depths, throughout a simulation. The kinematics of each participant (source, target, receiver) is manually specified within FORTRAN subroutines, which are compiled to create an

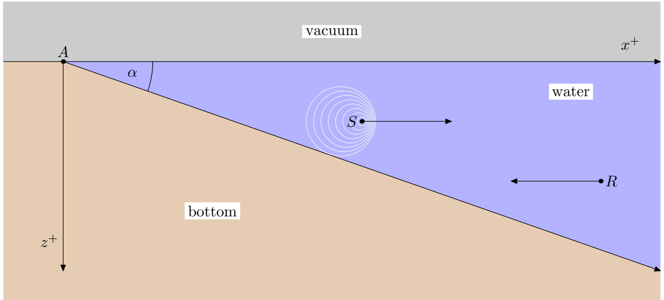

Fig. 6. The 2D wedge environment modelled within `WEDGE`.

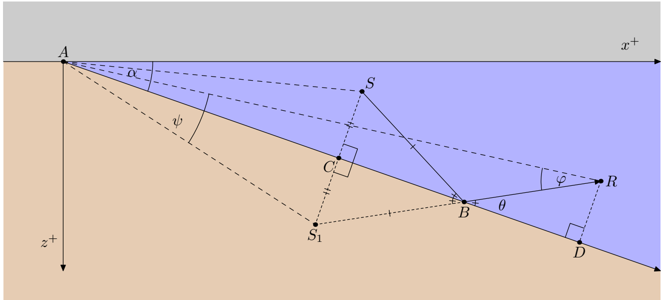

Fig. 7. The bottom (B) ray. The ray $\overrightarrow{SBR}$ strikes the bottom at B, and appears to come from a virtual source S_1, which is point S reflected about the bottom $\overrightarrow{AD}$. This figure is a companion to Fig. 8, and illustrates the geometry for S closer to A.

executable. First–order time derivatives of the x– and y–axis parametric equations of motion of each participant are also required to be encoded in FORTRAN subroutines, so that the exact Doppler shifts may be computed along each multipath and at each sampling instant. `DPRAY` synthesizes a received time series in the moving time frame of a receiver by a method of backtracking, locating where each source was when it transmitted energy received at a given instant of sampling. There will, in general, be different time delays for each different multipath, and the distribution of time delays may vary throughout a simulation. One of the goals of `DPRAY` is to accurately produce the correct Doppler shift, at all sampling instants, for each ray path throughout a simulation. Section V demonstrates the method of backtracking that is used in both `DPRAY` and `WEDGE`.

V. `WEDGE`

Fig. 6 shows a 2D beach model, consisting of a uniform fluid wedge (water) overlying a uniform solid basement. We assume a Cartesian (x, z) coordinate system, with origin A, where x is range (horizontal) and z is depth (vertical). Note that range is positive to the right of A, and depth is positive downwards. These conventions are indicated in Fig. 6 by the labels x^+ and z^+ on the positive range and depth axes, respectively. A more realistic 3D beach model would have a *shoreline*, the y axis, say, that is perpendicular to the (x, z) plane of Fig. 6 and which passes through point A. `WEDGE` only deals with acoustic energy that propagates in the plane $\{(x, y, z) : y = 0\}$ of that 3D model. The wedge has angle $0 < \alpha < \pi/2$.

A point monopole acoustic source S is located in the wedge, transmitting a complex unit–amplitude acoustic signal $s(t)$ with time variation of the form

$$s(t) = e^{-i(\omega_0 t + \varphi_0)}, \tag{66}$$

where $\omega_0 = 2\pi f_0$, f_0 is the rest frequency, in Hertz, t is time, in seconds, and φ_0 is the initial phase. This signal is sensed by an ideal point receiver, R, also in the wedge.

The motion of S is described in parametric form by

$$x_S(t) = x_S(0) + v_S t, \quad \text{and} \tag{67}$$
$$z_S(t) = z_S; \tag{68}$$

while the motion of R is described by

$$x_R(t) = x_R(0) + v_R t, \quad \text{and} \tag{69}$$
$$z_R(t) = z_R. \tag{70}$$

Both S and R remain at a fixed depth, z_S and z_R, respectively, and move at fixed speeds $0 \le |v_S| < c_1$ and $0 \le |v_R| < c_1$, respectively, where c_1 is the speed of sound in water. A negative velocity indicates motion towards the apex A: the velocity vectors illustrated in Fig. 6 satisfy $0 < v_S < c_1$ and $-c_1 < v_R < 0$.

`WEDGE` computes the acoustic pressure observed at R at times j/f_s, for $j \in \{1, 2, \ldots, N\}$, where f_s is the sample rate, in Hertz, and N is the required number of samples. Fig. 6 illustrates a train of circular wavefronts emitted by S. Note the compression occurring in the direction of motion of S, giving rise to the *Doppler effect*. `WEDGE` uses geometric acoustics (ray tracing), based on the *method of images*, to accurately model the Doppler effect resulting from motion of S and/or R, along all multipaths, at all sample times j/f_s.

Fig. 7 shows an acoustic multipath $\overrightarrow{SBR}$, consisting of the separate ray paths $\overrightarrow{SB}$ followed by $\overrightarrow{BR}$. Ray $\overrightarrow{SBR}$ bounces off the bottom interface (the 'bottom') at a point B, on its way from S to R. We shall refer to $\overrightarrow{SBR}$ as the 'B' ray, where B stands for bottom bounce.

At time t, R was at the coordinates $(x_R(t), z_R(t))$, as given by (69) and (70). The B–ray component of the sound energy received by R at time t departed from S at the instant $t - \tau_{\mathrm{B}}$, where $\tau_{\mathrm{B}} > 0$. At time $t - \tau_{\mathrm{B}}$, S was at the coordinates $(x_S(t - \tau_{\mathrm{B}}), z_S(t - \tau_{\mathrm{B}}))$, as given by (67) and (68) with $t - \tau_{\mathrm{B}}$ in place of t. From the perspective of R, τ_{B} is the propagation delay (at time t) of sound energy along the B ray.

Let θ_S be the angle of depression of the radial vector $\overrightarrow{AS}$ of S below the surface interface $\{(x, z) : x > 0, z = 0\}$, where $0 < \theta_S < \alpha < \frac{\pi}{2}$. Likewise, let θ_R be the angle of depression of the radial vector $\overrightarrow{AR}$ of R below the surface, where $0 < \theta_R < \alpha < \frac{\pi}{2}$. From the kinematic models (67)–(70)

we have

$$\theta_S = \tan^{-1}\left(\frac{z_S(t-\tau_{\rm B})}{x_S(t-\tau_{\rm B})}\right), \quad \text{and} \tag{71}$$

$$\theta_R = \tan^{-1}\left(\frac{z_R(t)}{x_R(t)}\right). \tag{72}$$

At the receiver R, the ray $\overrightarrow{BR}$ appears to come from a *virtual* source S_1 located in the bottom, where S_1 is the reflection of S about the bottom line $z = x\tan\alpha$. By Snell's Law, the ray $\overrightarrow{SBR}$ strikes the bottom at point B such that the angles of incidence ($\measuredangle SBC$) and reflection ($\measuredangle RBD$) are the same, where C and D are the feet of S and R, respectively, on the bottom.

From symmetry, triangles SBC and S_1BC are congruent, with common side $\overline{CB}$ on line $\overrightarrow{AD}$. Thus $\measuredangle S_1BC = \measuredangle SBC = \measuredangle RBD = \theta$, say. As C, B and D are on the same straight line $\overrightarrow{AD}$, $\measuredangle CBS_1 + \measuredangle S_1BD = \pi$, so that $\measuredangle S_1BD = \pi-\theta$. Hence $\measuredangle S_1BD + \measuredangle RBD = (\pi-\theta)+\theta = \pi$, and therefore S_1, B and R are collinear.

From symmetry, the radial distances AS and AS_1 are equal, to r_S, say, where

$$r_S = \sqrt{[x_S(t-\tau_{\rm B})]^2 + [z_S(t-\tau_{\rm B})]^2}. \tag{73}$$

Likewise, denote the radial distance AR by r_R, where

$$r_R = \sqrt{[x_R(t)]^2 + [z_R(t)]^2}. \tag{74}$$

From Fig. 7 we see that r_S and r_R are the lengths of sides $\overline{AS_1}$ and $\overline{AR}$, respectively, of triangle AS_1R. Let r be the length of the third side, $\overline{S_1R}$. Note that

$$\begin{aligned} r &= S_1R \\ &= S_1B + BR \\ &= SB + BR, \end{aligned} \tag{75}$$

so that r is also the length of the B–ray $\overrightarrow{SBR}$.

Applying the cosine rule in triangle AS_1R we have

$$r^2 = r_R^2 + r_S^2 - 2r_Rr_S\cos\psi, \tag{76}$$

where, referring to Fig. 7, we have

$$\begin{aligned} \psi &= \measuredangle S_1AB + \measuredangle BAR \\ &= \measuredangle SAB + \measuredangle BAR \\ &= (\alpha-\theta_S) + (\alpha-\theta_R) \\ &= 2\alpha - \theta_S - \theta_R. \end{aligned} \tag{77}$$

Finally, from simple physics (distance = speed × time) we note that the distance along the B ray is also given by $r = c_1\tau_{\rm B}$, and thus we have the following transcendental equation in the unknown $\tau_{\rm B}$:

$$\begin{aligned} c_1^2\tau_{\rm B}^2 &= r_R^2 + r_S^2 - 2r_Rr_S\cos(2\alpha-\theta_S-\theta_R) \\ &= [x_R(t)]^2 + [z_R(t)]^2 + [x_S(t-\tau_{\rm B})]^2 + [z_S(t-\tau_{\rm B})]^2 \\ &\quad - 2\sqrt{[x_R(t)]^2 + [z_R(t)]^2} \\ &\quad\times \sqrt{[x_S(t-\tau_{\rm B})]^2 + [z_S(t-\tau_{\rm B})]^2} \\ &\quad\times \cos(2\alpha-\theta_S-\theta_R). \end{aligned} \tag{78}$$

To find τ_B from (78) we fix the values of c_1, $x_R(0)$, v_R, z_R, $x_S(0)$, v_S, z_S, α and t and form the function $h(\tau_B)$, which is the difference between the left– and right–hand sides of (78), *viz.*

$$\begin{aligned} h(\tau_B) &= c_1^2\tau_{\rm B}^2 - [x_R(0)+v_Rt]^2 - z_R^2 \\ &\quad - [x_S(0)+v_S(t-\tau_B)]^2 - z_S^2 \\ &\quad + 2\sqrt{[x_R(0)+v_Rt]^2 + z_R^2} \\ &\quad\times \sqrt{[x_S(0)+v_S(t-\tau_B)]^2 + z_S^2} \\ &\quad\times \cos(\xi), \end{aligned} \tag{79}$$

where

$$\begin{aligned} \xi = 2\alpha &- \tan^{-1}\left(\frac{z_S}{x_S(0)+v_S(t-\tau_B)}\right) \\ &- \tan^{-1}\left(\frac{z_R}{x_R(0)+v_Rt}\right). \end{aligned} \tag{80}$$

`WEDGE` solves equation (79) using a root–finding technique. With fixed values for c_1, $x_R(0)$, v_R, z_R, $x_S(0)$, v_S, z_S, α and t, `WEDGE` computes $h(0)$ using an absolute lower bound $\tau_{\rm B} = 0$, and $h(1)$ at $\tau_{\rm B} = 1$. If the product $h(0)h(1) < 0$ then the true time delay $\tau_{\rm B}$ must lie within $(0,1)$ and the root–finding algorithm is called, returning an estimate $\tau_{\rm B}^*$ of $\tau_{\rm B}$.

If $h(0)$ and $h(1)$ are of the same sign, however, `WEDGE` computes $h(2)$ and the product $h(1)h(2)$. If $h(1)h(2) > 0$, then $h(4)$ and the product $h(2)h(4)$ are computed. This procedure is iterated over a sequence of intervals $(0,1)$, $(1,2)$, $(2,4)$ and so on, until an interval $\tau_{\rm B} \in (2^{n-1}, 2^n)$ is found that brackets a root, indicated by $h(2^{n-1})h(2^n) < 0$. In practice, this technique seems to work well, and appears suitable even for source and/or receiver speeds close to the speed of sound in water, c_1.

The angle φ in Fig. 7 is given from the sine rule in triangle AS_1R by

$$\frac{\sin\varphi}{AS_1} = \frac{\sin\psi}{S_1R} \tag{81}$$

so that, with $AS_1 = r_S$ and $S_1R = r$, we have

$$\begin{aligned} \varphi &= \sin^{-1}\left[\frac{r_S}{r}\sin\psi\right] \\ &= \sin^{-1}\left[\frac{r_S}{r}\sin(2\alpha-\theta_S-\theta_R)\right]. \end{aligned} \tag{82}$$

Once an estimated root $\tau_{\rm B}^*$ is available, r, r_S, θ_S and hence φ may be calculated.

Observe from Fig. 7 that angle RBD is exterior to triangle RAB, so that

$$\measuredangle RBD = \measuredangle ARB + \measuredangle BAR, \tag{83}$$

that is,

$$\theta = \varphi + \alpha - \theta_R. \tag{84}$$

Let $R_b(\theta)$ denote the complex reflection coefficient of a plane wave that strikes the bottom at a grazing angle of θ,

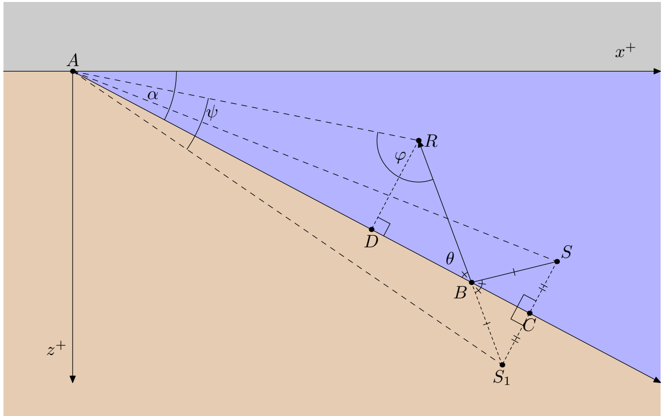

Fig. 8. The bottom (B) ray. This figure is a companion to Fig. 7, and illustrates the geometry for R closer to A.

where $0 < \theta \le \frac{\pi}{2}$. (Note that the grazing angle is measured *with respect to the sloping bottom*, so that a plane wave striking the bottom at the limiting grazing angle $\theta = 0$ is actually propagating parallel to the line $z = x \tan \alpha$. Conversely, a plane wave that strikes the bottom at normal incidence has a grazing angle $\theta = \pi/2$ and is propagating parallel to the line $z = -x \cot \alpha$.) Taking into account spherical spreading and bottom loss, then, and with the complex signal model (66), the B–ray contribution to the total coherent pressure received at R at time t is therefore

$$\frac{R_b(\theta)}{c_1 \tau_{\mathrm{B}}} s(t - \tau_{\mathrm{B}}) = \frac{R_b(\theta)}{c_1 \tau_{\mathrm{B}}} \exp\left(-i\left(\omega_0 (t - \tau_{\mathrm{B}}) + \varphi_0\right)\right). \tag{85}$$

Fig. 8 shows the B ray with the positions of S and R transposed from their positions in Fig. 7. We observe that the angle $\varphi = \measuredangle S_1 R A$ is now obtuse ($\frac{\pi}{2} < \varphi < \pi$), whereas the angle φ in Fig. 7 was acute ($0 < \varphi < \frac{\pi}{2}$). Note from Fig. 8 that the following identity holds in $\triangle ARB$:

$$\measuredangle BAR + \measuredangle ARB + \measuredangle RBA = \pi, \tag{86}$$

and so, with $\theta = \measuredangle RBA$,

$$\theta = \pi - (\varphi + \alpha - \theta_R), \tag{87}$$

which is the supplement of the result in (84). WEDGE automatically computes the appropriate value of θ, using either of (84) or (87), such that θ is in the interval $0 < \theta < \frac{\pi}{2}$.

The polar co-ordinates of the real source S and the virtual source S_1 are $(r_S, 2\pi - \theta_S)$ and $(r_S, 2\pi - (2\alpha - \theta_S))$, respectively (*cf.* Figs. 7, 8, (71), (73)). Thus S and S_1 lie on the same circle, centred on wedge apex A, with angular separation between S and S_1 being $2(\alpha - \theta_S)$.

In general, for a given receiver position $(x_R(t_j), z_R(t_j))$ and a given ray, the source S and each virtual source S_1, ..., S_m are arranged on the same circle. This circle is centred on the wedge apex A and has a radius equal to that of the radial distance of the source from A at the delayed time $t_j - \tau$, where $t_j = j/f_s$ is the time of sampling and $\tau = \tau(t_j)$ is the time delay for the given ray at time t_j. WEDGE simulates time series by including all of the finite number m of multipaths that exist at each sampling instant t_j, $j \in \{1, ..., N\}$.

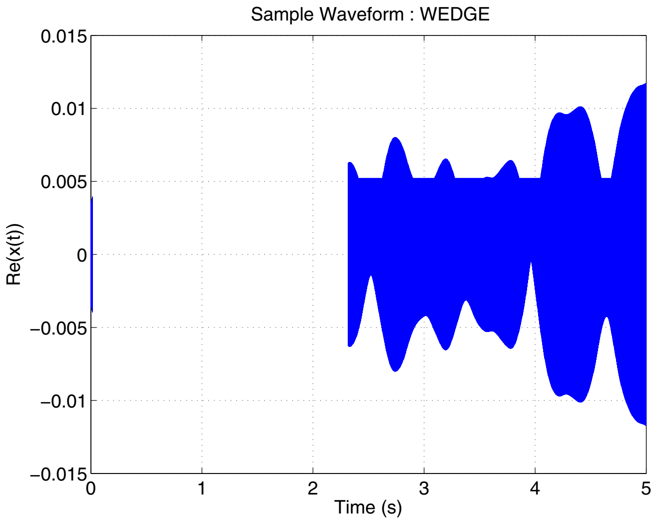

Fig. 9. Sample time series computed with WEDGE.

Fig. 9 shows the real part of a sample of time series data computed with WEDGE. The wedge angle was 2 degrees, and the solid basement was 'basalt', with the same parameters used for Fig. 5. The source was moving away from the wedge at depth $3\,\mathrm{m}$ and speed $10\,\mathrm{m{\cdot}s^{-1}}$, beginning at a horizontal range of $100\,\mathrm{m}$ from the wedge apex. The receiver was moving towards the wedge apex, at depth $10\,\mathrm{m}$ and speed $10\,\mathrm{m{\cdot}s^{-1}}$, beginning at range $1\,\mathrm{km}$. The source emitted a pure tone of frequency $1\,\mathrm{kHz}$ and 5 seconds of time series data was synthesized using a sampling frequency f_s of $16\,\mathrm{kHz}$.

REFERENCES

[1] P. C. Etter, *Underwater Acoustic Modelling and Simulation*, London: Spon Press, 2003.

[2] F. B. Jensen, W. A. Kuperman, M. B. Porter and H. Schmidt, *Computational Ocean Acoustics*, New York: Springer–Verlag, 2000.

[3] L. M. Brekhovskikh, *Waves in Layered Media*, 2nd ed., New York: Academic Press, 1980.

[4] G. V. Frisk, *Ocean and Seabed Acoustics*, Englewood Cliffs, New Jersey: P T R Prentice Hall, 1994.

[5] Ocean Acoustics Library. [Online]. URL: http://oalib.hlsresearch.com/.

[6] E. K. Westwood and P. J. Vidmar, "Eigenray finding and time series simulation in a layered–bottom ocean," *J. Acoust. Soc. Am.*, vol. 81, no. 4, pp. 912–924, Apr. 1987.

[7] G. V. Frisk, "Inhomogeneous waves and the plane–wave reflection coefficient," *J. Acoust. Soc. Am.*, vol. 66, no. 1, pp. 219–234, Jul. 1979.

[8] QUADPACK. [Online]. URL: http://www.netlib.org/quadpack/.

[9] H. Schmidt and F. B. Jensen, "An efficient numerical solution technique for wave propagation in horizontally stratified ocean environments", Memorandum SM-173, SACLANTCEN, North Atlantic Treaty Organization, La Spezia, Italy, 1984.

[10] OASES. [Online]. URL: http://acoustics.mit.edu/faculty/henrik/oases.html.

[11] M. A. Ainslie, "Plane–wave reflection and transmission coefficients for a three–layered elastic medium," *J. Acoust. Soc. Am.*, vol. 97, no. 2, pp. 954–961, Feb. 1995.

[12] D. Lévesque and L. Piché, "A robust transfer matrix formulation for the ultrasonic response of multilayered absorbing media," *J. Acoust. Soc. Am.*, vol. 92, no. 1, pp. 452–467, Jul. 1992.